

Comparison of methods that use whole genome data to estimate the heritability and genetic architecture of complex traits

Luke M. Evans^{1*}, Rasool Tahmasbi¹, Scott I. Vrieze², Gonçalo R. Abecasis³, Sayantan Das^{1,3}, Steven Gazal^{4,5}, Douglas W. Bjelland¹, Teresa R. de Candia¹, Haplotype Reference Consortium⁶, Michael E. Goddard^{7,8}, Benjamin M. Neale^{1,5}, Jian Yang^{1,9}, Peter M. Visscher⁹ and Matthew C. Keller^{1,10*}

Multiple methods have been developed to estimate narrow-sense heritability, h^2 , using single nucleotide polymorphisms (SNPs) in unrelated individuals. However, a comprehensive evaluation of these methods has not yet been performed, leading to confusion and discrepancy in the literature. We present the most thorough and realistic comparison of these methods to date. We used thousands of real whole-genome sequences to simulate phenotypes under varying genetic architectures and confounding variables, and we used array, imputed, or whole genome sequence SNPs to obtain 'SNP-heritability' estimates. We show that SNP-heritability can be highly sensitive to assumptions about the frequencies, effect sizes, and levels of linkage disequilibrium of underlying causal variants, but that methods that bin SNPs according to minor allele frequency and linkage disequilibrium are less sensitive to these assumptions across a wide range of genetic architectures and possible confounding factors. These findings provide guidance for best practices and proper interpretation of published estimates.

Narrow-sense heritability, h^2 , the proportion of a trait's phenotypic variance attributable to additive genetic variance, is a fundamental concept in quantitative genetics. In addition to being the central descriptor of the genetic bases of traits, h^2 determines the response to selection and the potential utility of individual genetic prediction^{1,2}. h^2 estimated in traditional designs using pedigrees or twins, \hat{h}_{PED}^2 , relies on strong assumptions about the causes of covariance between close relatives and can be biased to the degree these assumptions are unmet^{3,4}. Over the last 8 years, alternative 'SNP-based' methods⁵ have been developed to estimate h^2 using measured SNPs, denoted \hat{h}_{SNP}^2 . When estimated in samples of nominally unrelated individuals, \hat{h}_{SNP}^2 is unlikely to be confounded by common environmental or nonadditive genetic effects that increase similarity of close relatives and should reflect the proportion of phenotypic variation due to causal variants (CVs) tagged by SNPs. When common SNPs are used in the analysis, \hat{h}_{SNP}^2 is expected to be less than h^2 and \hat{h}_{PED}^2 because rare CVs are typically poorly tagged by common SNPs, and indeed \hat{h}_{SNP}^2 is substantially lower than \hat{h}_{PED}^2 for most complex traits in such analyses, with schizophrenia⁶ ($\hat{h}_{\text{SNP}}^2 \sim 0.23$ versus $\hat{h}_{\text{PED}}^2 \sim 0.8$) being a typical example.

More recently, imputed SNPs have been used to capture the effects of rarer CVs and to gain insight into the genetic architecture of traits, examine genetic networks and annotation classes, and test evolutionary hypotheses^{6–18}. For example, the substantial fraction of the variance in prostate cancer risk due to rare variants suggests that

negative selection has reduced the frequency of risk alleles¹⁸, and across a range of traits, young alleles explain more of the heritability than old alleles, suggesting widespread purifying selection^{13,14}. Whole-genome sequence (WGS) SNPs are likely to be increasingly used for such purposes in the future.

As SNPs in these analyses begin to more accurately reflect the density and frequency distributions of CVs, \hat{h}_{SNP}^2 should approach total h^2 , making it important to understand the factors that can bias \hat{h}_{SNP}^2 . Moreover, the proliferation of methods (Table 1) has led to discrepancies in estimates. For example, schizophrenia \hat{h}_{SNP}^2 has been reported as 0.56 (linkage disequilibrium (LD) score regression¹⁹) and as 0.23 (univariate genomic relatedness matrix residual maximum likelihood analysis (GREML)¹⁶). Recently, Speed et al.¹⁵ argued that typical assumptions about the relationships between SNP effect size, minor allele frequency (MAF), and LD are inaccurate and reported \hat{h}_{SNP}^2 values substantially higher than previous estimates under different assumptions. How should such discrepancies be interpreted? Under which conditions do biases exist across different methods, and when should researchers prefer one method over another? Answers to these questions are important, yet to date, comparisons across methods have been restricted to a small subset of methods in the primary papers they were introduced in, and have been compared across simulations that are unrealistic with respect to properties of real genomes. For example, simulating CVs from imputed genotypic data rather than measured WGS data¹⁵ can lead

¹Institute for Behavioral Genetics, University of Colorado, Boulder, CO, USA. ²Department of Psychology, University of Minnesota, Minneapolis, MN, USA.

³Center for Statistical Genetics, Department of Biostatistics, University of Michigan, Ann Arbor, MI, USA. ⁴Department of Epidemiology, Harvard T.H. Chan School of Public Health, Boston, MA, USA. ⁵Program in Medical and Population Genetics, Broad Institute of MIT and Harvard, Cambridge, MA, USA.

⁶A list of members and affiliations appears in the Supplementary Note. ⁷Faculty of Veterinary and Agricultural Science, University of Melbourne, Parkville, VIC, Australia. ⁸Agriculture Victoria, Bundoora, VIC, Australia. ⁹Institute for Molecular Bioscience and the Queensland Brain Institute, University of Queensland, Brisbane, QLD, Australia. ¹⁰Department of Psychology and Neuroscience, University of Colorado, Boulder, CO, USA.

*e-mail: luke.m.evans@colorado.edu; matthew.c.keller@gmail.com

Table 1 | Summary of commonly applied methods and a description of findings from simulations

Method	Description	Major assumptions	Simulation findings regarding \hat{h}_{SNP}^2	Computational issues
GREML-SC ⁵	Often called the GCTA approach. Originally applied to common array SNPs only. Estimates \hat{h}_{SNP}^2 , the amount of h^2 caused by CVs tagged by SNPs used to create the GRM.	(i) Genetic similarity is uncorrelated with environmental similarity; (ii) an infinitesimal model; (iii) SNP effects are normally distributed, independent of LD, and inversely proportionate to MAF ($\alpha = -1$).	Biased to the degree that the average LD among SNPs is different from the average LD between SNPs and CVs. This occurs in stratified samples and when MAF and LD distributions of SNPs do not match those of CVs.	Simple model tractable with large samples (>100,000).
GREML-MS ¹¹	The first multicomponent approach, usually applied by binning SNPs according to their MAF, annotation, or physical regions to explore genetic architecture.	Requires that the same assumptions of GREML-SC hold within each GRM.	Biased when CVs have generally higher or lower levels of LD than the SNPs used to make the GRM. Relatively large standard errors.	Run times and memory requirements higher than GREML-SC and increase as a function of the number of variance components estimated.
GREML-LDMS-R ⁷	A multicomponent approach that bins imputed SNPs by their MAF and regional LD.	Same as GREML-MS.	Use of regional LD scores can lead to biases when CVs have different LD on average compared to surrounding SNPs. Relatively large standard errors.	Same as GREML-MS.
GREML-LDMS-I	A multicomponent approach introduced here that bins imputed SNPs by their MAF and individual LD.	Same as GREML-MS.	Appears to be the least biased approach, even when traits have complex genetic architectures. Relatively large standard errors.	Same as GREML-MS.
LDAK-SC ^{15,20}	Introduced to account for redundant tagging of CVs by common SNPs. Recently modified to incorporate error due to imputation and to alter the MAF effect-size relationship.	Same as GREML-SC, except that allelic effects are a function of LD. Extended to assume that effects are also a function of imputation quality and weakly inversely proportionate to MAF ($\alpha = -0.25$).	Can correct for the overestimation observed in GREML-SC from redundant tagging of CVs, but otherwise about as biased as GREML-SC when assumptions are unmet, although the biases are sometimes in different directions.	Same as GREML-SC.
LDAK-MS ¹⁵	A multicomponent extension of LDAK-SC that bins SNPs by MAF.	Requires that the same assumptions of LDAK-SC hold within each GRM.	Less biased on average than LDAK-SC, but more biased than GREML-LDMS-I or -R. Relatively large standard errors.	Same as GREML-MS.
Threshold GRMs ²⁴	A multicomponent approach with two GRMs: the normal (unthresholded) GRM built from all SNPs and a second GRM with entries set to 0 if below a threshold. Conducted in samples that include close relatives.	Same as GREML-SC for the unthresholded GRM. Assumes no shared environmental influences among close relatives.	Estimates associated with unthresholded GRM similar to those of GREML-SC. When used in samples that include close relatives, the second GRM captures pedigree-associated variation but can be upwardly biased by shared environmental influences.	See GREML-SC.
LD score regression ¹⁹	Uses the slope from χ^2 (from GWAS) regressed on SNPs' LD scores to estimate the h^2 due to CVs in LD with common SNPs.	Infinitesimal model with allelic effects normally distributed.	Largely robust to confounding due to stratification and shared environmental influences. Estimates h^2 due to common CVs only, even when used on imputed or WGS data. Underestimates h^2 if the trait is not highly polygenic.	The most computationally efficient method of those compared and tractable for very large datasets.

to CVs with highly atypical levels of LD and therefore to conclusions about \hat{h}_{SNP}^2 that apply to genetic architectures unrepresentative of real traits.

Here we used thousands of fully sequenced genomes to simulate traits across different genetic architectures and degrees of population stratification, and we compared the performance of the most popular SNP heritability estimation methods using three different SNP types (array, imputed, and WGS). By simulating phenotypes from real WGS data rather than from simulated, array, or imputed SNPs, we were able to mimic patterns of LD and stratification found in real genomes and to include the effects of CVs down to a MAF of 0.0003. We then estimated heritability and the allelic spectra of

six complex traits in the UK Biobank. Our findings provide insight into the most important factors influencing, and best practices for estimating, \hat{h}_{SNP}^2 .

Results

Comparison of \hat{h}_{SNP}^2 across estimation methods under typical assumptions about CV effect sizes. For all methods described here other than LD score regression, evidence for \hat{h}_{SNP}^2 occurs to the degree to which the genome-wide average correlation between pairs of individuals i and j at measured SNPs, A_{ij} , is related to phenotypic similarity. A_{ij} values between all pairs of individuals are stored in an $n \times n$ genomic relationship matrix (GRM), used to estimate

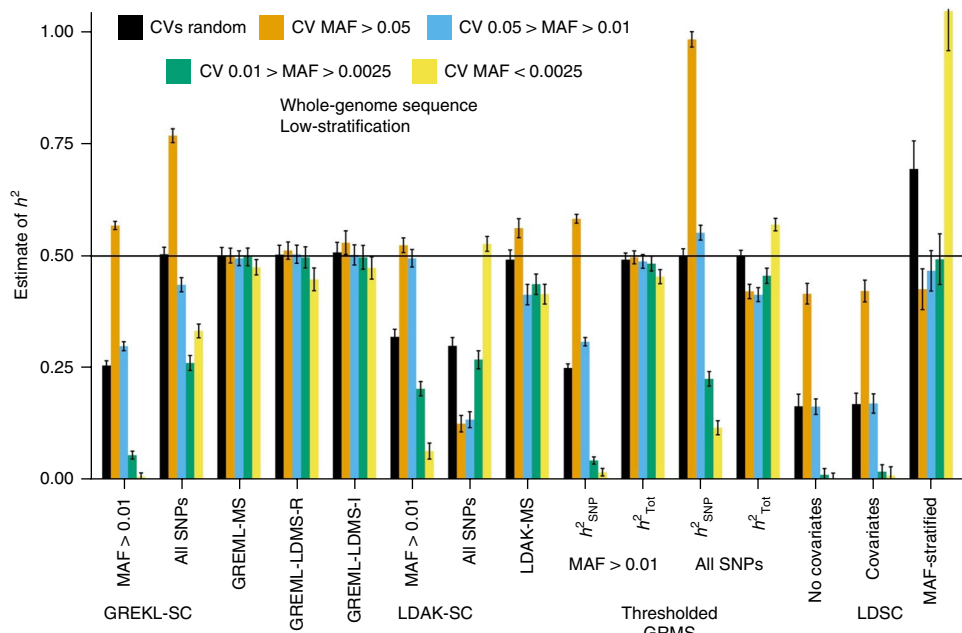


Fig. 1 | Comparison of heritability estimation methods. Mean \hat{h}_{SNP}^2 across 100 replicates from GRMs built from WGS SNPs in the least structured subsamples, $h_{\text{Total}}^2 = h_{\text{SNP}}^2 + h_{\text{BS}}^2$; LDSC is shown using no principal components (PCs) as covariates in GWAS, using PCs as covariates, or partitioned using PCs with MAF-stratification. Estimates are from samples of unrelated individuals (relatedness < 0.05) except for those from the Threshold GRM method, which included all individuals. Simulated (true) $h^2 = 0.5$. Colors represent the MAF range of the 1,000 randomly drawn CVs. See Methods for descriptions of each method, Supplementary Figs. for additional estimates, and Supplementary Table 2 for numerical results. Error bars represent 95% confidence intervals.

\hat{h}_{SNP}^2 with restricted maximum likelihood (REML). Such models can be fit using a single GRM ('single-component GREML')^{5,20} or by binning SNPs according to MAF, LD, and/or other annotations into multiple GRMs (multicomponent GREML)^{7,11}, akin to multiple regression and leading to one \hat{h}_{SNP}^2 per GRM, which can be summed to derive total \hat{h}_{SNP}^2 .

We used WGS data from the Haplotype Reference Consortium²¹ to mimic four levels of stratification found within Europe by varying the ancestry compositions of samples (each $n = 8,201$; see Methods). We simulated traits using 1,000 randomly chosen WGS CVs within five different MAF ranges under typical assumptions (CV effect sizes independent of LD and inversely proportionate to MAF, per-CV contribution to h^2 invariant across MAF). Later, we tested alternative assumptions. While all CVs are SNPs in our simulations (i.e., we did not simulate non-SNP CVs, such as repeat polymorphisms), we hereafter restrict our usage of 'SNPs' to denote the markers used to create GRMs and 'CVs' to denote underlying causal variants. We estimated h^2 using commonly applied methods (see Supplementary Note for additional methods) and used SNPs on a typical commercial platform (the UK Biobank Axiom array²²), SNPs imputed from an independent reference panel, or WGS SNPs to create GRMs. When WGS SNPs were used to create GRMs, CVs were necessarily included in the markers that created the GRMs, whereas this occurred sporadically for array and imputed SNPs. We simulated 100 phenotypes for each parameter combination and found the means of \hat{h}_{SNP}^2 and their empirical 95% confidence intervals across replicates. We did not simulate any phenotypic effects as a function of ancestry, and thus biases related to stratification in our results were due to the genotypic (for example, long-range LD), not environmental, effects of stratification.

We note that, in some contexts, it is useful to compare \hat{h}_{SNP}^2 to a corresponding population parameter, h_{SNP}^2 , which is defined as the true proportion of variance explained by the set of SNPs used in the analysis²³ and which in most cases is less than the full h^2 due

to imperfectly tagged CVs. However, such a formulation is cumbersome in the current context because h_{SNP}^2 changes across each combination of genetic architecture and SNP data type. Instead, in all cases we compare \hat{h}_{SNP}^2 to the full (simulated) h^2 , with the recognition that downward biases in \hat{h}_{SNP}^2 are expected when CVs are imperfectly tagged by (array and imputed) SNPs used in the analysis and that such underestimates do not necessarily reflect estimation problems. Because this expected underestimation does not apply to WGS data, and because these methods will be increasingly applied to WGS data in the future, in this section we focus primarily on results from WGS data; results from imputed SNPs (which were similar) and array SNPs (which were often dissimilar) are discussed briefly below but are presented in full in the Supplementary Note.

The most widely used estimation method, single-component GREML⁵ (GREML-SC, or the 'genome-wide complex trait analysis' (GCTA) approach¹⁵), underestimated h^2 when average CV MAF < average SNP MAF, such as when CVs were rare and array SNPs were analyzed, and overestimated h^2 when average CV MAF > average SNP MAF, such as when CVs were common and WGS SNPs were analyzed (Fig. 1, Supplementary Figs. 1–6, and Supplementary Tables 1–3). These biases are predictable based on SNP–SNP versus SNP–CV LD: when the mean LD between CVs and SNPs (r_{Q}^2) is less than the mean LD between all SNPs (r_{MM}^2), which occurs when CVs are on average rarer than SNPs, \hat{h}_{SNP}^2 underestimates h^2 , and vice versa when $r_{\text{Q}}^2 > r_{\text{MM}}^2$ (Supplementary Fig. 7)⁷. GREML-SC analyses using array SNPs led to modest overestimation of h^2 when CVs were common (Supplementary Fig. 1), presumably because array SNPs are chosen to maximally tag surrounding genomic regions. Stratification led to long-range tagging between ancestry-specific (rare) CVs and ancestry-informative common SNPs, which altered these biases. In the most stratified sample, average LD for very rare SNPs was higher than average LD for common SNPs (Supplementary Fig. 7), which led to

overestimation of h^2 when CVs were very rare and underestimation of common CV h^2 when using WGS or imputed variants (Supplementary Figs. 3–5). Controlling for ancestry principal components as fixed effects had no influence on these biases. Thus, stratification, CV MAF, and data type strongly influenced patterns of CV and SNP LD, leading to over- or underestimated h^2 using GREML-SC.

Speed et al. introduced an approach (LD-adjusted kinships or LDAK) to LD-weighted SNPs, to account for the redundant tagging of CVs by multiple SNPs, which can bias \hat{h}_{SNP} in certain situations²⁰. We limit discussion here to single-component LDAK (LDAK-SC) as originally described²⁰, and explore recent extensions of this model¹⁵ below with different simulations. As with GREML-SC, LDAK-SC estimates were highly sensitive to stratification, CV MAF, and SNP data type. When using common SNPs for the analysis (array, imputed, or WGS), LDAK-SC underestimated h^2 arising from rare CVs, but corrected the overestimation arising from common CVs observed with GREML-SC (Fig. 1 and Supplementary Figs. 1 and 2). However, when using all SNPs from WGS data, LDAK weighted SNPs inversely proportionally to their LD, resulting in near-zero weights for common SNPs and very high weights for rare SNPs (Supplementary Figs. 8 and 9). This led to underestimated h^2 when CVs were common and overestimated h^2 when CVs were very rare (Fig. 1 and Supplementary Fig. 4). This overweighting of rare SNPs appeared to exacerbate biases arising from stratification versus the unweighted (GREML-SC) approach (Supplementary Figs. 3–5). On the other hand, when all imputed SNPs were modeled in unstratified samples, LDAK appeared to provide decent estimates of h^2 (Supplementary Fig. 5), although results in the next section suggest that this was due to offsetting biases that happened to cancel out across this particular combination of parameters. Overall, the LDAK-SC results reiterate that GREML-SC models are highly sensitive to assumptions about genetic architecture.

We compared four multicomponent approaches: (i) GREML-MS⁷ (4 GRMs), which binned SNPs into four MAF categories; (ii) regional LD- and MAF-stratified GREML (GREML-LDMS-R)⁷ (16 GRMs), which binned SNPs by the MAF crossed by the average LD of SNPs in the surrounding ~200-kb region; (iii) individual LDMS GREML (GREML-LDMS-I; 16 GRMs), which we introduce here and which binned SNPs by MAF crossed by their individual levels of LD; and (iv) MAF-stratified LDAK (LDAK-MS)^{15,20} (4 GRMs), which binned SNPs by MAF and weighted them according to the LDAK model. There were no major differences between the results of the first three approaches: all provided roughly unbiased total \hat{h}_{SNP}^2 (the sum of \hat{h}_{SNP} from each GRM) when used on imputed or WGS data (Fig. 1 and Supplementary Figs. 1–5). The similarity of these estimates was anticipated in this set of simulations because CV effects were unrelated to LD, but below we demonstrate that GREML-LDMS-I provides the most robust estimates when this is not the case. LDAK-MS provided less biased \hat{h}_{SNP} than LDAK-SC but more biased \hat{h}_{SNP} than the other three multicomponent GREML methods when CVs were rare. Biased \hat{h}_{SNP} from LDAK-MS could occur because the simulation model does not match the LDAK assumption that CV effect sizes are a function of LD; we explore this issue below. In general, multicomponent models outperform single-component models because r_{QM}^2 is closer to r_{MM}^2 within narrower MAF and LD ranges, and therefore \hat{h}_{SNP} values associated with each partitioned GRM—and their sums—are likely to be approximately unbiased, consistent with previous work⁷. For similar reasons, these models were less biased in stratified samples than single-component models (Supplementary Figs. 3–5). However, the empirical standard errors of \hat{h}_{SNP} from GREML-LDMS-I were ~20–50% higher than those from GREML-LDMS-R, which were in turn ~100% higher than those from GREML-SC (Supplementary Figs. 10–12). Thus, multicomponent GREML models require large sample sizes (for example, $n > 30,000$) to be informative.

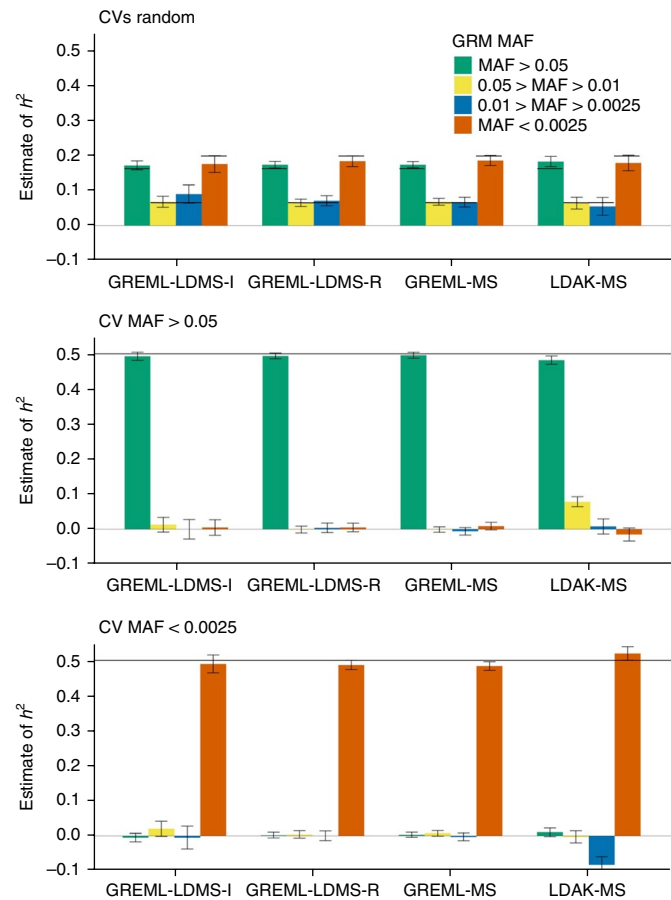


Fig. 2 | Partitioned heritability methods to explore allelic spectra of traits. Mean \hat{h}_{SNP}^2 for four MAF bins across 100 replicates from multicomponent approaches in unrelated individuals using WGS SNPs in the least structured subsample. Black horizontal lines are the true (simulated) h^2 values; note that in the top panel, the true h^2 values differ across MAF. See Methods for descriptions of each method, Supplementary Figs. for additional estimates, and Supplementary Table 4 for numerical results. Error bars represent 95% confidence intervals.

Zaitlen et al.²⁴ proposed a two-GRM approach to obtain \hat{h}_{PED}^2 and \hat{h}_{SNP}^2 in samples containing close relatives. The first GRM contains A_{ij} for all pairs of individuals, while A_{ij} values below a threshold, t (here $t=0.05$), are set to 0 in the second GRM. The first GRM contains information on sharing of CVs tagged by SNPs and is used to obtain \hat{h}_{SNP}^2 , while the second GRM only contains information from closely related individuals, reflecting sharing of CVs not tagged by SNPs, and is used to obtain $\hat{h}_{IBS>t}^2$, the additional h^2 captured by close relatives. The sum of $\hat{h}_{IBS>t}^2$ and \hat{h}_{SNP}^2 therefore provides an estimate of \hat{h}_{PED}^2 . In our simulations, \hat{h}_{PED}^2 was an unbiased estimate of h^2 across most situations examined (Supplementary Figs. 13 and 14). However, $\hat{h}_{IBS>t}^2$ and \hat{h}_{SNP}^2 were often severely over- or underestimated individually, depending on the CV MAF range and data type, with patterns of \hat{h}_{SNP} similar to those observed for GREML-SC. Thus, attempts to use this method to infer genetic architecture should be treated with caution. Moreover, as acknowledged by Zaitlen et al.²⁴ and demonstrated in additional simulations, \hat{h}_{PED}^2 may be biased upward when environmental factors cause similarity within nuclear or extended families (Supplementary Fig. 15).

LD score regression (LDSC) is an alternative, computationally efficient approach that estimates h^2 from the relationship between LD-tagging of individual SNPs and their expected genome-wide association study (GWAS) test statistics under an

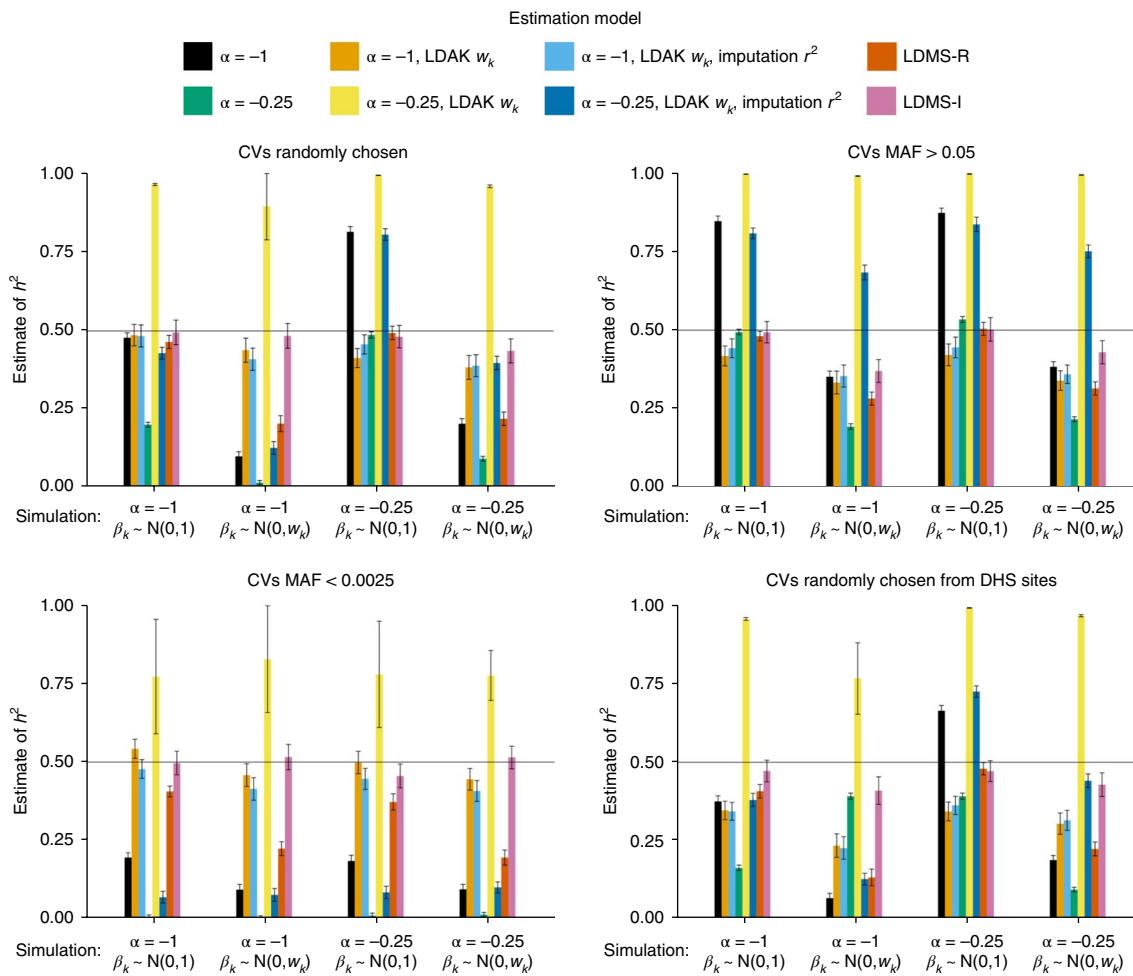


Fig. 3 | Influence of model assumptions using phenotypes simulated under alternative genetic architectures. Mean \hat{h}_{SNP}^2 across 100 replicates from GRMs built from imputed SNPs in the least structured subsamples across different model assumptions (bars) and different ways of simulating CVs (x axes). Each panel shows a different MAF range of the 1,000 randomly drawn CVs. DHS sites were randomly sampled without respect to MAF. Bar colors indicate the fitted model, with a single GRM used, except for the LDMS models, which used 16 GRMs ($\alpha = -1$) stratified by MAF and either regional (R) or individual SNP (I) LD scores. See Methods for descriptions of each method, Supplementary Figs. for additional estimates, and Supplementary Table 6 for numerical results. Error bars represent 95% confidence intervals.

infinitesimal model^{10,19}. Results from LDSC were similar when using array, imputed, or WGS SNPs (Fig. 1 and Supplementary Figs. 1, 2, and 16–18), as were estimates of the intercept, which reflect the contribution of stratification and cryptic relatedness to the GWAS test statistics (see Supplementary Note for further discussion of LDSC statistics). Across data types, LDSC generally underestimated h^2 by 5–10% when CVs were common. LDSC increasingly underestimated h^2 when CVs were rare, regardless of data type, because rare SNPs and CVs generally have very low LD scores. However, LDSC was largely immune to the genomic effects of stratification (see Supplementary Note), and we found no upward bias when unmodeled shared environmental effects were included in the simulations (Supplementary Fig. 15), suggesting that \hat{h}_{SNP}^2 from LDSC is robust to familial environmental effects and provides a reasonable estimate of the lower bound of h^2 tagged by common CVs.

We also simulated ascertained, case-control phenotypes applying the standard transformation to the liability scale²⁵. While the smaller sample size from ascertainment increased standard errors, patterns of \hat{h}_{SNP}^2 estimates across methods were similar to those found with continuous phenotypes (Supplementary Fig. 19), suggesting that our conclusions here apply to categorical outcomes.

Finally, multicomponent methods can also estimate h^2 across different annotations or different MAF bins (the ‘allelic spectra’ of traits). Multicomponent GREML approaches accurately estimated the allelic spectra when using WGS data (Fig. 2 and Supplementary Fig. 20). However, these approaches underestimated the contribution of very rare CVs by up to 20% using imputed data (Supplementary Fig. 21), due to the poorer imputation quality of rare SNPs, and substantially underestimated their contribution when using array SNPs (Supplementary Fig. 22) due to the low LD typically observed between array SNPs and rare CVs (Supplementary Tables 4 and 5).

Comparison of \hat{h}_{SNP}^2 models under alternative assumptions. Recent work has shown that, conditioning on MAF, SNPs with individually low levels of LD contribute disproportionately to the heritability of multiple complex traits¹³, suggesting that CV effects are not independent of their levels of LD. The simulations above assumed that CV effect sizes, β_k , were independent of LD and that rare CVs had, on average, larger effect sizes than common CVs, and therefore that the per-CV h^2 was invariant on average across MAF. This is achieved by applying an α of -1 , which governs the MAF effect-size relationship, and assuming $\beta_k \sim N(0, 1)$, the default scaling of GREML-SC, GREML-LDMS-R, and GREML-LDMS-I^{5,7}.

(see Methods). Recently, Speed et al.¹⁵ argued that less biased \hat{h}_{SNP}^2 estimates are obtained using a single-component model, but by assuming a higher contribution of common CVs (i.e., $\alpha = -0.25$), by assuming SNP effect sizes, w_k , are inversely proportionate to LD (Supplementary Figs. 8 and 9), and by weighting SNPs by imputation quality (r^2) (the LDAK model). Across numerous traits, they observed LDAK-SC-based \hat{h}_{SNP}^2 25–43% higher than \hat{h}_{SNP}^2 from GREML-SC and GREML-LDMS-R, as well as higher log-likelihoods from LDAK-SC models.

We compared the performance of these alternative assumptions of MAF, LD, and CV effect-size relationships with simulated phenotypes using CVs drawn from different MAF ranges under four different combinations of MAF effect-size ($\alpha = -1$ or -0.25) and LD effect-size ($\beta_k \sim N(0, 1)$ or $\beta_k \sim N(0, w_k)$) relationships. We also simulated phenotypes from two distinct, functionally relevant genetic architectures. We first simulated phenotypes with CVs randomly chosen from all DNase-I hypersensitivity sites, which have systematically lower LD¹⁷. Second, we simulated phenotypes using the empirically estimated, LD-dependent effect size distribution, $\beta_k \sim N(0, \tau_k)$, where τ_k was estimated across 31 traits using partitioned LDSC¹³ (see Methods). This latter simulation is particularly important because the functional, LD-dependent genetic architecture it used was independent of the assumptions made in the GREML and LDAK models used in estimation. Because LDAK-SC was intended to be used on imputed data, our primary results below are based on imputed SNPs, but results from WGS data are also presented in the Supplementary Note.

\hat{h}_{SNP}^2 from single-component models, including GREML-SC and LDAK-SC, were highly sensitive to model assumptions about MAF and LD effect-size relationships, as well as to differences between CV and SNP MAF distributions (Fig. 3, Supplementary Figs. 23 and 24, and Supplementary Tables 6 and 7). Moreover, in simulations with empirically derived genetic architectures¹³ ($\beta_k \sim N(0, \tau_k)$), both GREML-SC and LDAK-SC (Fig. 4 and Supplementary Fig. 25 and 26) were highly biased. On the other hand, multicomponent GREML models were much more robust to model misspecification (Figs. 3 and 4 and Supplementary Figs. 23–28). In particular, when we binned SNPs by their individual LD scores (GREML-LDMS-I), \hat{h}_{SNP}^2 estimates were robust across every genetic architecture we investigated (Fig. 3), including when CV effect sizes were drawn from the empirically estimated genetic architectures (Fig. 4). Across all genetic architectures and all data types investigated, GREML-LDMS-I had the lowest absolute bias of any method (Fig. 5). This suggests that particular assumptions regarding MAF and LD effect-size relationships are mitigated by the use of multiple-component models.

Of note, log likelihood was not a reliable indicator of degree of bias. Speed et al.¹⁵ argued that higher log-likelihood assuming $\alpha = -0.25$ than $\alpha = -1$ suggested that the former was more tenable. Across single-component models, which had the same number of predictors and therefore comparable log likelihoods, models with higher log likelihoods were typically less biased. However, we observed multiple cases in which negligible differences in log likelihood translated into large differences in bias, as well as situations in which models with higher average log likelihoods produced more biased results than models with lower average log likelihoods (Supplementary Figs. 23–26).

Heritability of complex traits in the UK Biobank. We applied seven approaches using imputed SNPs to six complex traits in the UK Biobank²⁶ (Fig. 6, Supplementary Figs. 29 and 30, and Supplementary Table 8). Differences in \hat{h}_{SNP}^2 across methods were consistent with our simulations. Estimates from single-component models were often higher than those from multicomponent models that bin SNPs by MAF and LD. For instance, the majority of height h^2 is attributable to common CVs²⁷, and GREML-SC and

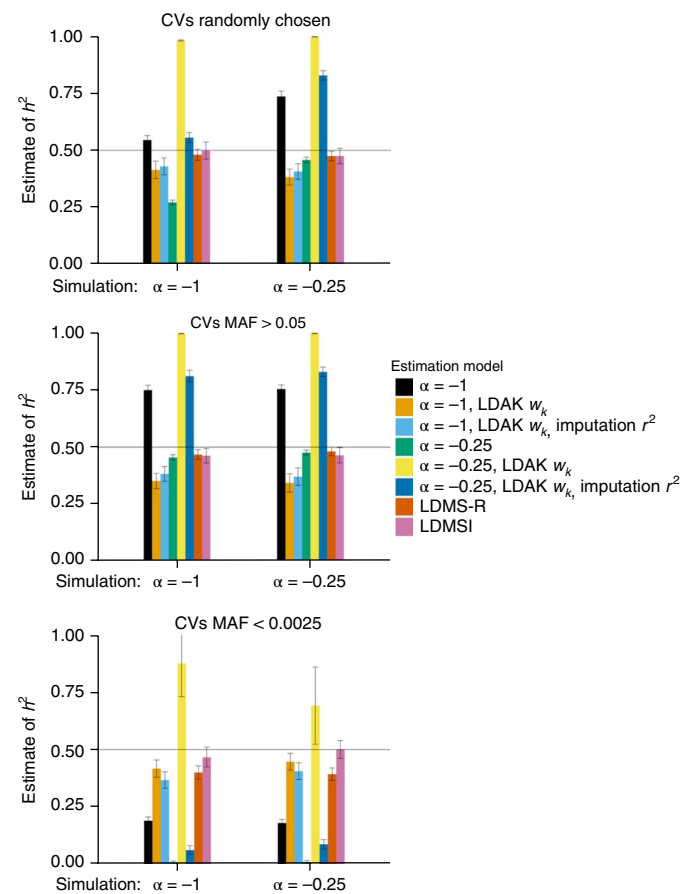


Fig. 4 | Influence of model assumptions using phenotypes simulated with LD-dependent genetic architecture. Mean \hat{h}_{SNP}^2 across 100 replicates from GRMs built from imputed SNPs in the least structured subsamples across different model assumptions (bars) and different ways of simulating CVs (x axes). CV effect sizes were simulated from $\sim N(0, \tau_k)$. Panels show different MAF ranges of the 1,000 randomly drawn CVs. Bar colors indicate the fitted model. See Methods for descriptions of each method, Supplementary Figs. for additional estimates, and Supplementary Table 6 for numerical results. Error bars represent 95% confidence intervals.

LDAK-SC \hat{h}_{SNP}^2 of height were unrealistically high ($>\hat{h}_{\text{PED}}^2$), which can occur when CVs are more common than SNPs used to build the GRM (Figs. 1, 3, and 4). On the other hand, estimates from multicomponent GREML were much more reasonable. These results provide context for understanding previously published estimates (see Supplementary Note), including those from Speed et al.¹⁵ showing higher LDAK \hat{h}_{SNP}^2 , and highlight the dangers of using single-component models that rely on strong assumptions about CV-effect sizes and MAF distributions.

Our results also suggest that the allelic spectra differ across the six traits, as estimated using GREML-LDMS-I, the most accurate approach in our simulations (Supplementary Fig. 31 and Supplementary Tables 9 and 10). For example, while the majority of height heritability was explained by common SNPs, 59% of fluid intelligence h^2 was due to rare CVs, with a total \hat{h}_{SNP}^2 (~0.35) that approached \hat{h}_{PED}^2 . Nevertheless, our simulations suggest that variance due to increasingly rare CVs was underestimated by ~20% for all traits, due to low imputation quality at lower MAF. This underestimate was probably more severe because the imputation reference panel (combined UK10K and 1,000 Genomes) used in the UK Biobank data was smaller by roughly half and less diverse than the reference panel used in our simulations.

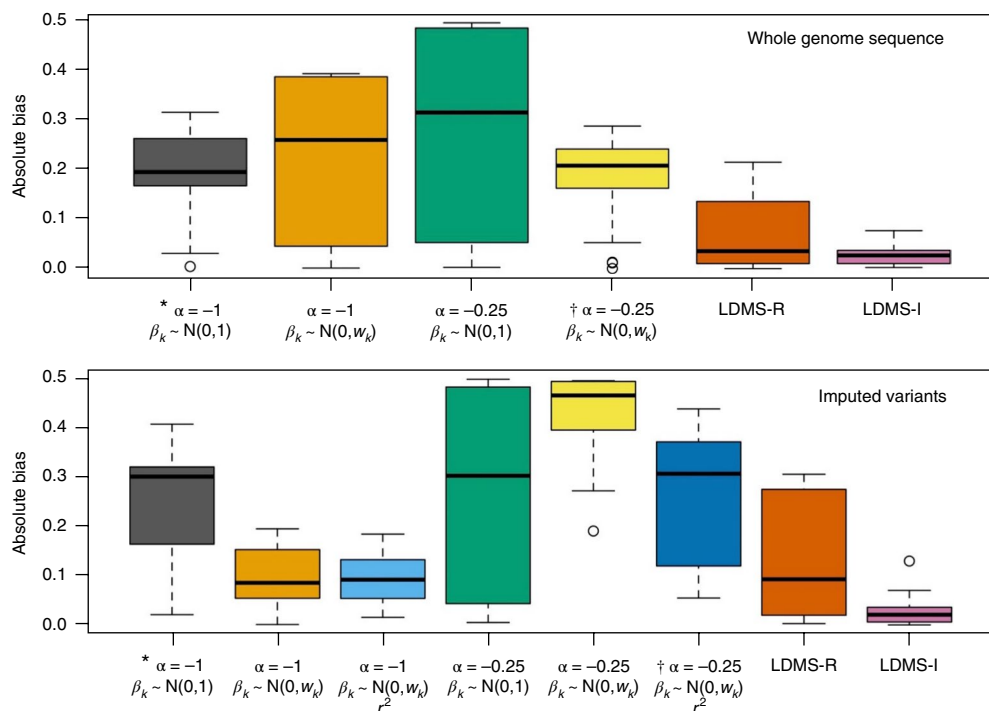


Fig. 5 | Bias of heritability estimates under different model assumptions. Boxplots of the absolute bias of heritability estimates ($|E(\hat{h}_{SNP}^2) - h^2|$) across all simulated phenotypes. Results are derived from Supplementary Figs. 24 and 26 using WGS data to estimate GRMs (top), and from Figs. 3 and 4 using imputed variants to estimate the GRMs (bottom). The x axis indicates the parameters for the estimation model; all used a single GRM except for LDMS, which used 16 GRMs ($\alpha = -1$) stratified by MAF and either regional (R) or individual SNP (I) LD score. *Typical GREML-SC parameters. †Typical LDAK-SC parameters. Boxplots show medians and interquartile ranges, with whiskers extending to $1.5 \times$ the quartiles and more extreme points shown for $n = 22$ (WGS) and 26 (imputed) mean estimates of heritability.

Discussion

We have demonstrated that estimates of h^2 and allelic spectra using SNP data can be biased in a number of ways that are sometimes difficult to foresee and depend strongly on a complex interplay between the method and type of data used in the analysis, trait genetic architecture, degree of sample stratification, shared environmental effects, and whether close relatives are included or excluded. Understanding how these factors influence \hat{h}_{SNP}^2 is crucial for proper interpretation of often-conflicting published estimates and for optimal design of future studies. Additional factors that we did not investigate might also influence the biases of \hat{h}_{SNP}^2 across methods, such as technical artifacts²⁸, environmental factors that co-vary with ancestry^{29,30}, CVs with MAF < 0.0003, or non-SNP CVs.

LD is central to the performance of all the methods compared here, particularly the LD among SNPs used to create the GRM and that between CVs and SNPs^{7,20}. Single-component models, such as GREML-SC and LDAK-SC, are highly sensitive to assumptions, especially when rare imputed or WGS SNPs are used to create the GRM. This is problematic given that it seems unlikely that a single set of assumptions will hold for all traits and across the entire allelic spectrum. Alternatively, multicomponent models that partition \hat{h}_{SNP}^2 across multiple LD and MAF bins provide the most robust estimates across the majority of contexts explored here, while simultaneously providing insight into the allelic spectra of complex traits. However, they are more computationally intensive and have higher standard errors than single-component models, and they require larger datasets to achieve reliable estimates. Nevertheless, such data are now at hand, and if the goal is to obtain the least biased estimates of h^2 or to estimate allelic spectra, we recommend using multicomponent GREML models. Even when using multicomponent approaches, h^2 is likely underestimated, but will improve as sample sizes increase and larger imputation panels and/or WGS data are used.

Based on the results of the present and previous studies, we summarize our suggestions for using SNPs to estimate h^2 and allelic spectra of complex traits. First, quality control of genetic data is crucial, particularly for case-control and/or multiple-cohort datasets, in which technical artifacts can inflate or deflate \hat{h}_{SNP}^2 ²⁸. Covariates (ancestry principal components, cohorts, plates, etc.) that might be confounded with genetic similarity should be included as fixed effects in GREML models and in the GWAS models for LDSC³¹. Related individuals may share common environmental and nonadditive genetic effects, upwardly biasing estimates of h^2 ; using unrelated individuals should provide estimates not inflated by such factors³².

Second, the model and data type used in the analysis strongly influence estimates. When genotype data are unavailable or impractical to use, LDSC provides a lower bound of the h^2 captured by common CVs and is unaffected by confounding due to stratification and the common environment. Single-component methods such as GREML-SC and LDAK-SC are highly sensitive to model misspecification, which can lead to severely biased estimates of heritability. Moreover, they are also sensitive to the effects of stratification, which are not mitigated by inclusion of ancestry covariates. We recommend these approaches only when sample sizes are small (for example, $n < 30,000$) and homogeneous. Multicomponent approaches with WGS or imputed SNPs provide the most accurate estimates of h^2 and allelic spectra across a range of genetic architectures and stratification levels. When using imputed data, SNPs should be imputed using the largest and most diverse reference panel possible (for example, Haplotype Reference Consortium²¹) in order to more reliably capture the effects of rare CVs. However, more GRMs lead to larger standard errors, necessitating larger sample sizes ($n > 30,000$). Of the multicomponent approaches, GREML-

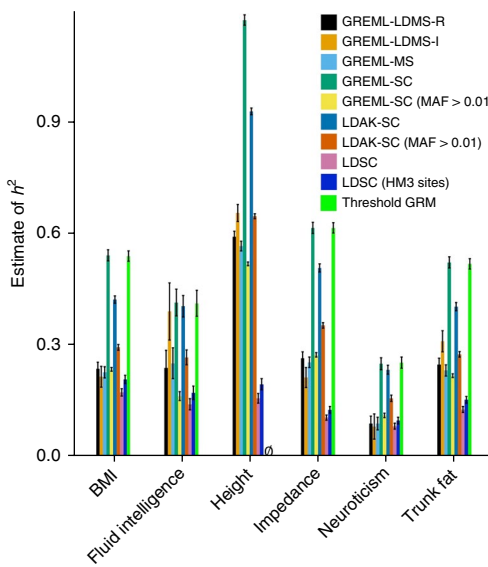


Fig. 6 | Estimated h_{SNP}^2 using multiple methods with imputed variants for six complex traits in the UK Biobank. MAF > 0.01 indicates that common SNPs were used to create the GRMs. \emptyset , information matrix was not invertible. HM3 indicates that only imputed HapMap3 sites were used in the LDSC analysis. Sample sizes as follows: height, $n=94,769$; body-mass index (BMI), $n=94,595$; impedance, $n=93,451$; trunk fat, $n=93,414$; fluid intelligence, $n=31,724$; neuroticism, $n=78,565$. See Supplementary Table 8 for numerical results. Error bars indicate s.e.m.

LDMS-I, which we introduce here and which bins SNPs by MAF and individual LD levels, appears to perform the best.

URLs. BOLT-REML, <https://data.broadinstitute.org/alkes-group/BOLT-LMM/>. GCTA, <http://cnsgenomics.com/software/gcta/#Overview>. Haplotype Reference Consortium, <http://www.haplotype-reference-consortium.org>. LDSC, <https://github.com/bulik/ldsc/wiki>. LDAK, <http://dougspeed.com/ldak/>. UK Biobank, <http://www.ukbiobank.ac.uk/>.

Methods

Methods, including statements of data availability and any associated accession codes and references, are available at <https://doi.org/10.1038/s41588-018-0108-x>.

Received: 15 March 2017; Accepted: 8 March 2018;

Published online: 26 April 2018

References

1. Tenesa, A. & Haley, C. S. The heritability of human disease: estimation, uses and abuses. *Nat. Rev. Genet.* **14**, 139–149 (2013).
2. Visscher, P. M., Hill, W. G. & Wray, N. R. Heritability in the genomic era—concepts and misconceptions. *Nat. Rev. Genet.* **9**, 255–266 (2008).
3. Keller, M. C. & Coventry, W. L. Quantifying and addressing parameter indeterminacy in the classical twin design. *Twin Res. Hum. Genet.* **8**, 201–213 (2005).
4. Eaves, L. J., Last, K. A., Young, P. A. & Martin, N. G. Model-fitting approaches to the analysis of human behaviour. *Heredity (Edinb.)* **41**, 249–320 (1978).
5. Yang, J. et al. Common SNPs explain a large proportion of the heritability for human height. *Nat. Genet.* **42**, 565–569 (2010).
6. Lee, S. H. et al. Estimating the proportion of variation in susceptibility to schizophrenia captured by common SNPs. *Nat. Genet.* **44**, 247–250 (2012).
7. Yang, J. et al. Genetic variance estimation with imputed variants finds negligible missing heritability for human height and body mass index. *Nat. Genet.* **47**, 1114–1120 (2015).
8. Hyde, C. L. et al. Identification of 15 genetic loci associated with risk of major depression in individuals of European descent. *Nat. Genet.* **48**, 1031–1036 (2016).
9. Okbay, A. et al. Genetic variants associated with subjective well-being, depressive symptoms, and neuroticism identified through genome-wide analyses. *Nat. Genet.* **48**, 624–633 (2016).
10. Finucane, H. K. et al. Partitioning heritability by functional annotation using genome-wide association summary statistics. *Nat. Genet.* **47**, 1228–1235 (2015).
11. Yang, J. et al. Genome partitioning of genetic variation for complex traits using common SNPs. *Nat. Genet.* **43**, 519–525 (2011).
12. Loh, P.-R. et al. Contrasting genetic architectures of schizophrenia and other complex diseases using fast variance-components analysis. *Nat. Genet.* **47**, 1385–1392 (2015).
13. Gazal, S. et al. Linkage disequilibrium-dependent architecture of human complex traits shows action of negative selection. *Nat. Genet.* **49**, 1421–1427 (2017).
14. Zeng, J. et al. Signatures of negative selection in the genetic architecture of human complex traits. *Nat. Genet.* <https://doi.org/10.1038/s41588-018-0101-4> (2018).
15. Speed, D., Cai, N., Johnson, M. R., Nejentsev, S. & Balding, D. J. Reevaluation of SNP heritability in complex human traits. *Nat. Genet.* **49**, 986–992 (2017).
16. Lee, S. H. et al. Genetic relationship between five psychiatric disorders estimated from genome-wide SNPs. *Nat. Genet.* **45**, 984–994 (2013).
17. Gusev, A. et al. Partitioning heritability of regulatory and cell-type-specific variants across 11 common diseases. *Am. J. Hum. Genet.* **95**, 535–552 (2014).
18. Mancuso, N. et al. The contribution of rare variation to prostate cancer heritability. *Nat. Genet.* **48**, 30–35 (2016).
19. Bulik-Sullivan, B. K. et al. LD score regression distinguishes confounding from polygenicity in genome-wide association studies. *Nat. Genet.* **47**, 291–295 (2015).
20. Speed, D., Hemani, G., Johnson, M. R. & Balding, D. J. Improved heritability estimation from genome-wide SNPs. *Am. J. Hum. Genet.* **91**, 1011–1021 (2012).
21. McCarthy, S. et al. A reference panel of 64,976 haplotypes for genotype imputation. *Nat. Genet.* **48**, 1279–1283 (2016).
22. Bycroft, C. et al. Genome-wide genetic data on ~ 500,000 UK Biobank participants. Preprint at *bioRxiv* <https://doi.org/10.1101/166298> (2017).
23. Yang, J., Zeng, J., Goddard, M. E., Wray, N. R. & Visscher, P. M. Concepts, estimation and interpretation of SNP-based heritability. *Nat. Genet.* **49**, 1304–1310 (2017).
24. Zaitlen, N. et al. Using extended genealogy to estimate components of heritability for 23 quantitative and dichotomous traits. *PLoS Genet.* **9**, e1003520 (2013).
25. Lee, S. H. et al. Estimation of SNP heritability from dense genotype data. *Am. J. Hum. Genet.* **93**, 1151–1155 (2013).
26. Sudlow, C. et al. UK Biobank: an open access resource for identifying the causes of a wide range of complex diseases of middle and old age. *PLoS Med.* **12**, e1001779 (2015).
27. Wood, A. R. et al. Defining the role of common variation in the genomic and biological architecture of adult human height. *Nat. Genet.* **46**, 1173–1186 (2014).
28. Lee, S. H., Wray, N. R., Goddard, M. E. & Visscher, P. M. Estimating missing heritability for disease from genome-wide association studies. *Am. J. Hum. Genet.* **88**, 294–305 (2011).
29. Browning, S. R. & Browning, B. L. Population structure can inflate SNP-based heritability estimates. *Am. J. Hum. Genet.* **89**, 191–193 (2011). author reply 193–195.
30. Goddard, M. E., Lee, S. H., Yang, J., Wray, N. R. & Visscher, P. M. Response to Browning and Browning. *Am. J. Hum. Genet.* **89**, 193–195 (2011).
31. Price, A. L., Zaitlen, N. A., Reich, D. & Patterson, N. New approaches to population stratification in genome-wide association studies. *Nat. Rev. Genet.* **11**, 459–463 (2010).
32. Zhu, Z. et al. Dominance genetic variation contributes little to the missing heritability for human complex traits. *Am. J. Hum. Genet.* **96**, 377–385 (2015).

Acknowledgements

We thank D. Speed (University College London) for providing LDAK5. We thank the Keller and Vrieze lab groups, the Institute for Behavioral Genetics, N. Wray, A. Price, and S. Caron for helpful comments. This work was supported by NIH grant R01MH100141 (to M.C.K.), NHMRC grants 1078037 (to P.M.V.) and 1113400 (to P.M.V. and J.Y.), Sylvia & Charles Viertel Charitable Foundation Senior Medical Research Fellowship (to J.Y.), and NIH grants R01DA037904 and R01HG008983 (to S.V.). This work used the Janus supercomputer, which is supported by the National Science Foundation (award number CNS-0821794), the University of Colorado Boulder, the University of Colorado Denver,

and the National Center for Atmospheric Research. The Janus supercomputer is operated by the University of Colorado Boulder. We thank the participants of the individual Haplotype Reference Consortium cohorts. This research has been conducted using the UK Biobank Resource.

Author contributions

L.M.E. and M.C.K. conceived and designed the study. L.M.E. performed the statistical analyses and simulations. R.T., S.I.V., S.G., G.R.A., S.D., D.W.B., T.R.d.C., M.E.G., B.M.N., J.Y., and P.M.V. provided statistical support. The Haplotype Reference Consortium, G.R.A., and S.D. contributed to data collection and management. L.M.E. and M.C.K. wrote the manuscript with participation of all authors.

Competing interests

The authors declare no competing interests.

Additional information

Supplementary information is available for this paper at <https://doi.org/10.1038/s41588-018-0108-x>.

Reprints and permissions information is available at www.nature.com/reprints.

Correspondence and requests for materials should be addressed to L.M.E. or M.C.K.

Publisher's note: Springer Nature remains neutral with regard to jurisdictional claims in published maps and institutional affiliations.

Methods

Samples and population structure. We simulated continuous phenotypes derived from WGS data in the Haplotype Reference Consortium (HRC)²¹. The HRC comprises ~32,500 individuals from multiple WGS studies, with called genotypes at all sites with minor allele count ≥ 5 . We had access to a subset (Supplementary Note) of 21,500 individuals with genotype calls at 38,913,048 biallelic SNPs. This large WGS dataset allowed phenotype simulation with differing genetic architectures under realistic patterns of LD structure, stratification, and relatedness.

The HRC is mainly composed of individuals with European ancestry. To reduce the effects of worldwide stratification, we identified European individuals using principal components analysis (PCA). We used `flashpca`³³ on 133,603 MAF- and LD-pruned SNPs (`plink2`³⁴ commands `-maf 0.05 -indep-pairwise 1000 400 0.2`) and extracted the first ten PCs. We used the 1,000 Genomes individuals in the HRC as anchor points for ancestry and identified 19,478 individuals of European descent, including individuals of Finnish and Sardinian ancestry using k -means clustering in R³⁵ (Supplementary Fig. 32).

To identify subsets of these 19,478 individuals spanning different levels of genetic heterogeneity, we reran PCA with only these individuals, then identified four increasingly homogenous subgroups within them using k -means clustering (Supplementary Fig. 33 and Supplementary Note). We sampled an equal number of individuals from each subset at a relatedness cutoff of 0.1 ($n = 8,201$) and also identified individuals with relatedness less than 0.05 within each group ($n = 7,792$; $n = 8,115$; $n = 8,129$; and $n = 8,186$ for the four subsamples) to examine how relatedness and stratification influence \hat{h}_{SNP}^2 estimates.

Simulation of phenotypes and whole genome data types. To assess how different methods performed on a range of genetic architectures, we simulated phenotypes from CVs drawn randomly from five MAF ranges from the WGS data: common (MAF ≥ 0.05), uncommon ($0.01 \leq \text{MAF} < 0.05$), rare ($0.0025 \leq \text{MAF} < 0.01$), very rare ($0.0003 \leq \text{MAF} < 0.0025$), and all SNPs that had a minor allele count (MAC) ≥ 5 (MAF ≥ 0.0003). We generated phenotypes from 1,000 CVs from the model $y_i = g_i + e_p$, where $g_i = \sum X_{ik}\beta_k$ and $X_{ik} = (z_{ik} - 2p_k)[2p_k(1 - p_k)]^{\alpha/2}$, where z_{ik} was the genotype, coded as 0, 1, or 2 of individual i at the k th CV, p_k was the MAF within a population subset, and β_k was the k th allelic effect size, drawn from $\sim N(0, 1)$. In these simulations, we used $\alpha = -1$, assuming larger average effect sizes for rarer SNPs. The g_i values were standardized and added to residual error drawn from $\sim N(0, (1 - h^2)/h^2)$ for $h^2 = 0.5$. A total of 100 replicated phenotypes were simulated for each CV MAF range and for each of the four population stratification subsets. Note that simulations did not include any ancestry (i.e., PC) effects, and thus stratification-driven biases were due to the genotypic (for example, long-range LD) effects of stratification.

To simulate ascertained case-control phenotype data in samples with some or low stratification (Supplementary Fig. 33b,c), we converted the continuous phenotypes simulated above to dichotomous case-control data using a prevalence of 20% ($k = 0.2$). We then combined the cases with an equal number of randomly sampled controls to simulate ascertained datasets, which reduced sample sizes (~40% of the continuous trait data). Note that this altered sample size reduces the genetic variance for phenotypes derived from rarer CVs. We transformed estimates of h^2 to the liability scale using the transformation described in Lee et al.²⁵.

To simulate array, imputed, and WGS data types, we first extracted from the WGS data SNP positions corresponding to a widely used commercially available genotyping array, the UK Biobank Affymetrix Axiom array (the array SNP dataset). We then imputed genome-wide variants using these Axiom SNPs and independent HRC samples as a WGS reference panel (the imputed dataset). Finally, we used the HRC WGS data directly (the WGS dataset). See Supplementary Note for details of each dataset. MAF distributions of the different data types for two of the structure subsamples are shown in Supplementary Fig. 34.

Heritability estimation methods tested. We briefly describe our implementation of the most commonly used methods to estimate h^2 and partition genetic variation using genome-wide data (see Supplementary Note for descriptions of and results from additional, less commonly used methods). For all methods except LDSC (described below), we generated GRMs following the standard procedures of each method, and estimated \hat{h}_{SNP}^2 using GCTA³⁶. In all models, variance component estimates were unconstrained (for example, by using the `-reml-no-constraint` option of GCTA) and included 20 PCs (10 from worldwide PCA and 10 from the specific subsample PCA) and sequencing cohort as fixed effects.

Single-component GREML (GREML-SC). Yang et al.⁵ introduced the single-component approach using a mixed-effects model, with GRM entries:

$$A_{ij} = \frac{1}{m} \sum_k^m \frac{(x_{ik} - 2p_k)(x_{jk} - 2p_k)}{2p_k(1 - p_k)} \quad (1)$$

where m is the number of SNPs, x_{ik} is the genotype (coded as 0, 1, or 2) of individual j at the k th locus, and p_k is the MAF of the k th locus. The variance of the phenotypes is

$$\text{var}(\mathbf{y}) = \mathbf{A}\sigma_v^2 + \mathbf{I}\sigma_e^2 \quad (2)$$

where the variance explained by the SNPs (σ_v^2) and error variance (σ_e^2) are estimated using restricted maximum likelihood (REML) implemented in the GCTA package³⁶. The proportion of the total variance explained by all SNPs is then a measure of heritability ($\hat{h}_{\text{SNP}}^2 = \sigma_v^2 / (\sigma_v^2 + \sigma_e^2)$). Typically, the set of m SNPs used to build the GRM is the set of SNPs with MAF ≥ 0.01 (hereafter ‘common SNPs’) and unrelated individuals (relatedness ≤ 0.05). We compared this typical approach to one using all SNPs with MAC ≥ 5 (hereafter ‘all SNPs’) in each particular stratification subsample and for each data type (note that ~9.5% of Axiom array positions have MAF < 0.01 in our sample), as well as to an approach using less stringent relatedness thresholds (relatedness < 0.10 and no relatedness threshold). For analyses that used no relatedness threshold, inclusion of close relatives increased our sample sizes to $n = 9,916$; $n = 8,701$; $n = 8,715$; and $n = 8,506$ for the samples with most, some, low, and least stratification, respectively (Supplementary Fig. 33).

MAF-stratified GREML (GREML-MS). \hat{h}_{SNP}^2 is expected to be a biased estimate of h^2 when using the GREML-SC method when the MAF distribution of the CVs does not match the MAF distribution of SNPs used to generate the GRM¹¹. Stratifying SNPs into MAF bins in a multiple GRM GREML approach can mitigate this bias and can partition \hat{h}_{SNP}^2 into that explained by different SNP MAF bins, lending insight into the allelic spectra of complex traits^{6,7}. For each data type, we applied this approach using four MAF bins, matching the CV MAF bins used for phenotype simulation.

LD- and MAF-stratified GREML (GREML-LDMS-R and GREML-LDMS-I).

Extending the GREML-MS method to account for different levels of LD throughout the genome, Yang et al.⁷ introduced an approach (originally termed GREML-LDMS but which we term GREML-LDMS-R here) that stratifies SNPs jointly by their MAF and regional LD scores, defined as the sum of r^2 between the focal SNP and all other SNPs in a 200-kb sliding window. We estimated LD scores using the default settings in GCTA (200-kb block size with a 100-kb overlap), and stratified SNPs into LD score quartiles (see Yang et al.⁷ for details). This resulted in 16 GRMs (4 MAF bins \times 4 LD bins) and therefore 16 values of \hat{h}_{SNP}^2 , which were summed to derive total \hat{h}_{SNP}^2 . SNPs with individually low levels of LD contribute disproportionately to the heritability for multiple complex traits, particularly low LD SNPs in regions of high LD¹³. Because these results suggest individual rather than regional LD levels influence heritability, we developed and compared results from an alternative approach (GREML-LDMS-I) that stratified by individual (rather than regional) SNP LD scores, again binning SNPs by LD quartiles and four MAF bins, for a total of 16 GRMs.

Single- and multicomponent LD-adjusted kinships (LDAK-SC and LDAK-MS). Speed et al.²⁰ noted that because LD varies across the genome, CVs in regions of high LD receive disproportionate weight by equation (1) above. The original LDAK²⁰ approach weights SNPs according to individual LD, potentially correcting for the bias introduced when there is variation in how well CVs are tagged by SNPs, and assumes standard MAF-CV effect size scaling ($\alpha = -1$). We used LDAK²⁰ to estimate these LD-weighted GRMs, which first thins SNPs in very high LD to reduce redundant tagging, then estimates SNP weights, w_k , that are inversely proportional to their average LD with other SNPs. We also applied the MAF-stratified approach described above, but using LDAK weights (LDAK-MS). For the single-component model (LDAK-SC), we used all SNPs (MAC ≥ 5) as well as only common SNPs (MAF ≥ 0.01) to build the GRM for each data type. For the MAF-stratified approach, following recommendations in the LDAK documentation, we estimated SNP weights over the union of all SNPs (MAC ≥ 5), and then computed GRMs for each MAF class separately. We then applied the multiple GRM method with these LDAK-weighted GRMs to estimate \hat{h}_{SNP}^2 using GCTA. Results from the first set of simulations (Figs. 1 and 2) come from the traditional LDAK approach described above; results from the second set of simulations (Figs. 3–5) come from the updated LDAK approach described in the section below (Simulation of data and comparison of \hat{h}_{SNP}^2 under alternative assumptions about CV effect sizes).

Extended genealogy with thresholded GRMs. Zaitlen et al.²⁴ introduced a method to simultaneously obtain \hat{h}_{SNP}^2 and \hat{h}_{PED}^2 by using two GRMs in a sample containing close relatives. The first GRM contains all A_{ij} , whereas the second GRM sets A_{ij} values below a threshold, t , to 0. The first GRM, therefore, contains information on allele sharing of (mostly common) variants in unrelated and related individuals (estimating \hat{h}_{SNP}^2), while the second only contains information from closely related individuals (estimating $\hat{h}_{\text{IBS},>p}^2$ following Zaitlen et al.²⁴). We tested two relatedness thresholds ($t \leq 0.05$ and $t \leq 0.1$) for the second GRM. The sum of $\hat{h}_{\text{IBS},>p}^2$ and \hat{h}_{SNP}^2 provides an estimate of total h^2 , similar to \hat{h}_{PED}^2 with all the same potential biases that exist in \hat{h}_{PED}^2 from designs that use close relatives. By necessity, all analyses using this approach included close relatives, which could lead to confounding between genetic and environmental similarity if shared environmental effects are not modeled^{37,38}. Indeed, Zaitlen et al.²⁴ argue that such shared environmental effects were the likely cause of higher \hat{h}_{PED}^2 estimates among relatives who shared an environment through cohabitation (for example, half-siblings) compared to equally

related relatives that did not share a cohabitation environment (for example, grandparents and grandchildren). We therefore assessed whether h_{SNP}^2 and h_{PED}^2 estimates from this method (as well as from GREML-SC and LDSC) were biased when extended family shared environmental effects were present but unmodeled in samples of closely related individuals (see Supplementary Note).

LD score regression (LDSC). LDSC uses a different approach to estimate the heritability tagged by common CVs. Rather than estimating relatedness within a sample for use in mixed-model GREML analysis, LDSC regresses GWAS test statistics (χ^2) on SNPs' LD scores, which reflect the degree to which each SNP is correlated with surrounding SNPs^{10,19}. For a polygenic model, the expected GWAS test statistic of SNP j , χ_j^2 , is

$$E[\chi_j^2 | l_j] = N(h_{\text{SNP}}^2)l_j/M + Na + 1 \quad (3)$$

where N is the sample size, M is the number of SNPs, l_j is the LD score ($= \sum_k r_{jk}^2$) measuring the tagging of surrounding variants by SNP j , and a is a measure of confounding biases arising from stratification and cryptic relatedness. Thus, regressing GWAS test statistics on per-SNP LD scores allows for both estimation of h_{SNP}^2 and assessing the degree of confounding or polygenicity of a trait¹⁹. Bulik-Sullivan et al.¹⁹ argue that LDSC provides unbiased estimates of h^2 tagged by common SNPs regardless of whether GWAS test statistics are estimated with or without controlling for ancestry, environmental covariates, or relatedness. Here we estimated GWAS test statistics using plink2 without controlling for ancestry covariates or for ancestry covariates (20 PCs and sequencing cohort as above). We used the ldsc package with default parameters (see “URLs”) to perform LDSC. We calculated LD scores for all SNPs using WGS data, including common and rare SNPs. As recommended by Bulik-Sullivan et al.¹⁹, we used unrelated individuals (relatedness ≤ 0.05) and only common SNPs to perform the regression itself, because the relationship between the GWAS χ^2 and LD score is unclear for rare (MAF < 0.01) SNPs. We examined the relationship among h_{SNP}^2 , the intercept, the mean χ^2 value, and the genomic control inflation factor, λ_{GC} (see Supplementary Note).

LDSC can also be used to partition heritability among annotations¹⁰. We applied this approach using the four MAF bins described above. Because our MAF bins included very rare SNPs, for this MAF-stratified LDSC, we used GWAS test statistics from all SNPs (MAF ≥ 0.0003 , using the -not-5–50 flag in the ldsc package) while controlling for covariates as above.

Simulation of phenotypes and comparison of h_{SNP}^2 under alternative assumptions about CV effect sizes. We tested the LDAK-SC, GREML-SC, and GREML-LDMS-R and -I methods on phenotypes emulated under alternative assumptions about CV effect sizes to determine the degree to which the methods were robust to model misspecification. To simulate phenotypes under alternative effect size assumptions, in the low-stratification sample only (Supplementary Fig. 33c), we varied the MAF effect-size relationship ($\alpha = -1$ or -0.25) and the effect size distribution ($\beta_k \sim N(0,1)$ or $\sim N(0, w_k)$, where w_k is the LDAK weight of the k th CV estimated from the WGS data, which is inversely proportional to the SNP LD score (Supplementary Figs. 8 and 9)). When $\beta_k \sim N(0,1)$ and $\alpha = -1$, this model is the same as above and as previously described¹. WGS CVs were drawn randomly from common SNPs (MAF > 0.05), very rare SNPs (MAF < 0.0025), all SNPs (MAF ≥ 0.0003), or randomly from all DHS sites (systematically lower LD¹⁷), annotated for all UK10K SNPs with MAC ≥ 2 . Note that, in Speed et al.¹⁵, effect sizes, β_k , are also assumed to be proportionate to the imputation quality scores (r^2). Because we were simulating CVs from WGS data rather than imputed variants, we did not include the r^2 term for simulating CV effect sizes.

Additionally, we simulated phenotypes using an independent LD architecture derived from the 75-annotation baseline-LD model described in ref. ¹³, which contains coding, conserved, DHS and other functional annotations, ten MAF bins, and six LD-related annotations modeling multiple LD-related architectures (including predicted allele age, recombination rate, and CpG-content). For these simulations, we annotated 20,678,452 SNPs with allele count greater or equal than 2 in 3,567 UK10K unrelated individuals, and modeled the variance of the k th SNP, τ_k , proportional to $\sum_{c=1}^{75} a_c(k)\theta_c$, where $a_c(k)$ was the continuous value annotations of CV k for annotation c and θ_c was the per-SNP contribution of one unit of the annotation a_c to the heritability. We used the values of θ_c estimated with stratified LDSC on 31 independent traits¹³ and constrained θ_c to be positive. Finally, as θ_c and stratified LDSC hold only for common SNPs, we rescaled the variance of all τ_k so that the heritability explained by the four rarest of the ten MAF bins (delimited by 0, 0.1%, 0.5%, 1%, and 5% boundaries) were equal to the expected variance of the bin ($= \sum (p_k(1-p_k))^{1+\alpha}$, where $\alpha = -0.28$, as estimated by Loh et al.¹²). We then simulated phenotypes as described above with effect sizes β_k drawn from $\sim N(0, \tau_k)$.

We compared estimates from models applying different assumptions of α and β_k . The traditional GREML-SC, GREML-LDMS-R, and GREML-LDMS-I estimate GRMs using $\alpha = -1$ and $\beta_k \sim N(0,1)$, while the updated LDAK-SC model of Speed et al.¹⁵ uses $\alpha = -0.25$ and $\beta_k \sim N(0, w_k)$, as well as weighting SNPs by imputation r^2 . To test these assumptions, we estimated GRMs using either $\alpha = -1$ or -0.25 and either weighting by LDAK weights or not. For imputed data, we also weighted SNP contributions to the GRM by imputation r^2 . For GREML-LDMS-R and -I, we used $\alpha = -1$ and no LDAK or imputation r^2 weighting.

Heritability of complex traits in the UK Biobank. We estimated heritability for six continuous phenotypes in the initial release of the UK Biobank²⁶ ($n \sim 150,000$) using the most commonly applied methods (Fig. 6). To reduce the effects of stratification, we used individuals of European ancestry (Supplementary Fig. 33). To estimate the GRMs, we separately used directly genotyped Axiom array positions as well as imputed genome-wide SNPs with IMPUTE info score ≥ 0.3 . See Supplementary Table 8 for the list of all methods we applied, and see Supplementary Note for additional methods and details.

Reporting Summary. Further information on experimental design is available in the Nature Research Reporting Summary linked to this article.

Data availability. Data are from the Haplotype Reference Consortium (<http://www.haplotype-reference-consortium.org/>) and the UK Biobank (<http://www.ukbiobank.ac.uk/>) and can be accessed through those resources.

References

33. Abraham, G. & Inouye, M. Fast principal component analysis of large-scale genome-wide data. *PLoS One* **9**, e93766 (2014).
34. Chang, C. C. et al. Second-generation PLINK: rising to the challenge of larger and richer datasets. *Gigascience* **4**, 7 (2015).
35. R Core Team. *R: a Language and Environment for Statistical Computing*. (R Foundation for Statistical Computing, Vienna, Austria, 2015).
36. Yang, J., Lee, S. H., Goddard, M. E. & Visscher, P. M. GCTA: a tool for genome-wide complex trait analysis. *Am. J. Hum. Genet.* **88**, 76–82 (2011).
37. Xia, C. et al. Pedigree- and SNP-associated genetics and recent environment are the major contributors to anthropometric and cardiometabolic trait variation. *PLoS Genet.* **12**, e1005804 (2016).
38. Zuk, O., Hechter, E., Sunyaev, S. R. & Lander, E. S. The mystery of missing heritability: Genetic interactions create phantom heritability. *Proc. Natl Acad. Sci. USA* **109**, 1193–1198 (2012).

Life Sciences Reporting Summary

Nature Research wishes to improve the reproducibility of the work we publish. This form is published with all life science papers and is intended to promote consistency and transparency in reporting. All life sciences submissions use this form; while some list items might not apply to an individual manuscript, all fields must be completed for clarity.

For further information on the points included in this form, see Reporting Life Sciences Research. For further information on Nature Research policies, including our data availability policy, see Authors & Referees and the Editorial Policy Checklist.

► Experimental design

1. Sample size

Describe how sample size was determined.

Our work was based on consortium data (HRC & UK Biobank); we therefore did not determine the sample size of the initial samples. In our simulations, we were interested in varying the amount of stratification in the samples, and in the least stratified subsample, this left 8,201 individuals, which represents the maximum sample size in the smallest group. We then randomly chose the same number of individuals from each other subsample to avoid confounding sample size differences with stratification. (P30, L481-497).
In the UK Biobank, we again attempted to maximize our sample size, within the constraint of maintaining relative homogeneity of the sample. We restricted the analyses to a relatively homogeneous subset, using UK Biobank-identified individuals of European ancestry to avoid stratification confounding our heritability estimates. (P43, L778-787).
These were the maximum possible sample sizes, given the consortium data we had access to. Given the expected standard errors, which roughly matched the empirical standard errors from simulation, these sample sizes (~30,000-95,000 for each of UK Biobank traits) were sufficient to provide small enough standard errors for interpretation.

2. Data exclusions

Describe any data exclusions.

Our study was restricted to sets of individuals of European ancestry, because this allowed the greatest sample size while limiting the effects of stratification.
In the UK Biobank sample, we excluded individuals with poor quality and those whose self-reported and genetic sex conflicted.

3. Replication

Describe whether the experimental findings were reliably reproduced.

For each simulation, we used 100 replicates. We used these for estimation of means and 95% confidence intervals. Of these 100 independent replicates, a small proportion did not converge, with the exact numbers presented in the Supplementary Tables. These failed because the information matrix was not invertible.

4. Randomization

Describe how samples/organisms/participants were allocated into experimental groups.

We used PCA to initially group individuals (P30, L481-497 & P43, L778-787). Within the HRC data, we randomly down-sample individuals to the same number (8201) within the stratification subsamples as described in #1 above.

5. Blinding

Describe whether the investigators were blinded to group allocation during data collection and/or analysis.

We identified groups via either K-means clustering and 1,000 Genomes population assignments, or using the UK Biobank-provided ancestry information. These groupings were intentionally done to minimize confounding effects of stratification while maximizing the possible sample sizes.

Note: all studies involving animals and/or human research participants must disclose whether blinding and randomization were used.

6. Statistical parameters

For all figures and tables that use statistical methods, confirm that the following items are present in relevant figure legends (or the Methods section if additional space is needed).

n/a Confirmed

- The exact sample size (n) for each experimental group/condition, given as a discrete number and unit of measurement (animals, litters, cultures, etc.)
- A description of how samples were collected, noting whether measurements were taken from distinct samples or whether the same sample was measured repeatedly.
- A statement indicating how many times each experiment was replicated
- The statistical test(s) used and whether they are one- or two-sided (note: only common tests should be described solely by name; more complex techniques should be described in the Methods section)
- A description of any assumptions or corrections, such as an adjustment for multiple comparisons
- The test results (e.g. p values) given as exact values whenever possible and with confidence intervals noted
- A summary of the descriptive statistics, including central tendency (e.g. median, mean) and variation (e.g. standard deviation, interquartile range)
- Clearly defined error bars

See the web collection on statistics for biologists for further resources and guidance.

► Software

Policy information about availability of computer code

7. Software

Describe the software used to analyze the data in this study.

The principal software used in this study was GCTA v1.26, available at

<http://cnsgenomics.com/software/gcta/index.html#Overview>.

Other analyses were performed using LDAK5 (provided by Doug Speed), PLINK2, BOLT-REML v2.3.1, LDSC v1, flashpca-1.1.2.1, minimac3, shapeit v2.r837.

URLs are detailed in the manuscript in individual method descriptions in the online methods and in the URLs section.

For all studies, we encourage code deposition in a community repository (e.g. GitHub). Authors must make computer code available to editors and reviewers upon request. The *Nature Methods* guidance for providing algorithms and software for publication may be useful for any submission.

► Materials and reagents

Policy information about availability of materials

8. Materials availability

Indicate whether there are restrictions on availability of unique materials or if these materials are only available for distribution by a for-profit company.

The data used were from the Haplotype Reference Consortium, a limited-access dataset (www.haplotype-reference-consortium.org) and the UK Biobank, available to researchers (<http://www.ukbiobank.ac.uk/>). No new data were collected for this study. They are also referenced in the Data Availability statement with their URLs.

9. Antibodies

Describe the antibodies used and how they were validated for use in the system under study (i.e. assay and species).

No antibodies were used.

10. Eukaryotic cell lines

a. State the source of each eukaryotic cell line used.

No eukaryotic cell lines were used.

b. Describe the method of cell line authentication used.

No eukaryotic cell lines were used.

c. Report whether the cell lines were tested for mycoplasma contamination.

No eukaryotic cell lines were used.

d. If any of the cell lines used in the paper are listed in the database of commonly misidentified cell lines maintained by ICLAC, provide a scientific rationale for their use.

No eukaryotic cell lines were used.

► Animals and human research participants

Policy information about studies involving animals; when reporting animal research, follow the ARRIVE guidelines

11. Description of research animals

Provide details on animals and/or animal-derived materials used in the study.

No animals used.

Policy information about studies involving human research participants

12. Description of human research participants

Describe the covariate-relevant population characteristics of the human research participants.

This study used previously collected data as described at <http://www.ukbiobank.ac.uk/> and www.haplotype-reference-consortium.org. We did not directly perform research on human participants.

As described above in points 1,2,4,&5, we restricted analyses to the largest available, reasonably homogeneous subset, which was of European ancestry. Fifteen ancestry PCs, age, age squared, assessment centre, batch, TDI, sex, and educational attainment were included as covariates in analyses of the UK Biobank data.

For simulations using the HRC, again restricting analyses to the largest available, reasonably homogeneous subset as described in points 1,2,4,&5, we applied twenty ancestry PCs and cohort as covariates in analyses.